Nano Carbons 2024; 2(1): 381.
Original Research Article

Vibration analysis of functionally graded carbon nanotubes reinforced composite nanoplates

Dang Van Hieu[1,2,*], Nguyen Thi Kim Thoa[3]

[1] *Faculty of Mechanical Engineering and Mechatronics, PHENIKAA University, Hanoi 12116, Vietnam*

[2] *A&A Green Phoenix Group JSC, PHENIKAA Research and Technology Institute (PRATI), No. 167 Hoang Ngan, Trung Hoa, Cau Giay, Hanoi 11313, Vietnam*

[3] *Department of Mechanics, Thai Nguyen University of Technology, Thainguyen 24000, Vietnam*

*** Corresponding author:** Dang Van Hieu, hieu.dangvan@phenikaa-uni.edu.vn

ARTICLE INFO

Received: 1 December 2023
Accepted: 18 January 2024
Available online: 19 February 2024

doi: 10.59400/nc.v2i1.381

ABSTRACT: This work presents the analytical analysis for free linear vibration behavior of functionally graded-carbon nanotubes reinforced composite (FG-CNTRC) nanoplates in the framework of nonlocal strain gradient theory (NSGT) and the first-order shear deformation plate theory (FSDPT). The nanoplate is considered made of a mixture of an isotropic polymer matrix and reinforced carbon nanotubes (CNTs). Four different distributions of CNTs are examined including uniformly distributed and FG reinforcements (FG-O, FG-X, and FG-V). The governing equations of motion are established based on the Hamilton's principle. The closed-form analytical solution for the natural frequency of FG-CNTRC nanoplates with simply supported all edges is carried out by using the Navier-type solution. The impact of some key parameters on the natural frequencies of FG-CNTRC nanoplates is also studied and discussed. The result shows that FG-CNTRC nanoplates reveal the softening- or hardening-stiffness effects depending on the relationship between the nonlocal parameter and the material length scale parameter. The aspect ratios of FG-CNTRC nanoplates, the volume fraction, and the distribution pattern of CNTs have also an important impact on the vibration behavior of FG-CNTRC nanoplates.

KEYWORDS: nonlocal strain gradient; nanoplate; free vibration; nanotubes; reinforcement; first-order shear deformation

1. Introduction

Possessing remarkable mechanical, thermal, and electrical properties, CNTs are known as excellent reinforcements for polymer composites[1]. The theoretical and experimental research reported that CNTs possess an extremely high elastic modulus greater than 1 TPa and tensile strength 10–100 times higher than the strongest steel; in a vacuum, CNTs have thermal stability up to 2800 °C; and CNTs have thermal conductivity about twice as high as diamond, electric-current-carrying capacity 1000 times higher than copper wires[1]. Research activities on behaviors and properties of CNTs have been investigated by many scientists in recent years. The concept of FG materials was developed first by Shen[2] for the nanocomposite plates reinforced by CNTs with low volume fraction. The material properties of FG-CNTRC plates were assumed to be graded in the thickness direction, which can be estimated through a micromechanical model in which the CNT efficiency parameters are estimated by matching the elastic modulus of CNTRCs observed from the molecular dynamics (MD) simulation results with the numerical results obtained from the rule of mixture[2]. This idea was further developed

by Shen and his colleagues for beam and plate models to examine the mechanical behaviors of these structures[3–5]. Two types of CNTRC structures including uniformly distributed (UD) and FG reinforcements (FG-O, FG-X, and FG-V), were proposed by the authors. Zhu et al.[6] used the FSDPT in conjunction with the NSGT to examine the bending and free linear vibration behaviors of FG-CNTRC plates by employing the finite element method (FEM). A comprehensive analysis was reported by Daikh et al.[7] to study the bending and buckling behaviors of FG-CNTRC plates under thermal environments. And especially, the mechanical behaviors of FG-CNTRC structures including beams, plates, and shells were reviewed by Liew and his co-authors in their paper[8].

As the main part in electrically or magnetically actuated models such as micro-/nano-electromechanical systems (MEMS/NEMS)[9], the mechanical behaviors of micro-/nano-sized beams and plates are increasingly receiving research attention[10]. Studies have shown that the mechanical behavior of these small-sized structures is governed by the size-dependent effect. Due to the absence of length scale parameters, the classical elasticity theory (CET) is not suitable for modeling micro-/nano-sized structures. To overcome this limitation of the CET, some non-classical elasticity theories have been proposed in which length scale parameters are incorporated. It can be mentioned as the nonlocal elasticity theory (NET) introduced by Eringen[11,12], in which the size-dependent effect can be captured by the presence of nonlocal parameters. From a different perspective, the strain gradient theory (SGT) proposed by Mindlin et al.[13,14] and the modified couple stress theory (MCST) proposed by Yang et al.[15], which can capture the size-dependent effect through material length scale parameters. And recently, both the nonlocal and material length scale parameters have been integrated by Lim et al.[16] into a generalized non-classical elasticity theory called the NSGT. These non-classical elasticity theories have been used very effectively to describe the mechanical behaviors of micro/nano-sized structures[10]. Based on the NET and Mindlin's plate theory (MPT), the free linear vibration of FG-CNTRC nanoplates was investigated by Shahriari et al.[17]. Gia Phi et al.[18] employed the NSGT to examine the nonlinear vibration response of FG-CNTRC microbeams with piezoelectric layers in thermal environments. The static and dynamic stability behaviors of multilayer FG-CNTRC nanoplates based on the NSGT and 3D kinematic shear deformation plate theory were reported by Daikh et al.[19] using Galerkin method. Hung et al.[20] investigated the bending and free linear vibration characteristics of FG-CNTRC microplates based on the SGT and MPT using Isogeometric approach.

In this work, the authors present an analytical analysis of the free linear vibration problem of FG-CNTRC nanoplates in the framework of the NSGT and FSDPT. The material properties of FG-CNTRC nanoplates with different distributions of CNTs are estimated using the extended rule of mixture. Closed-form solutions for the free linear vibration problem of FG-CNTRC nanoplates with simply supported all edges are provided. Numerical simulations are conducted to assess the reliability of the present results and evaluate the influence of several key parameters, including nanoplate's aspect ratios, length scale parameters, CNT volume fraction, and distribution types of CNTs, on the free linear vibration response of FG-CNTRC nanoplates.

2. Mathematical formulations

2.1. Functionally graded-carbon nanotubes reinforced composite nanoplate

An FG-CNTRC nanoplate with length a, width b, and thickness h is considered as in **Figure 1**. The coordinate system ($Oxyz$) is chosen as shown in **Figure 1**, in which the origin of coordinate system O is located at the corner of the middle surface of the nanoplate. The nanoplate is assumed to be composed

of an isotropic polymer matrix reinforced by CNTs along the length direction of the nanoplate (*x*-direction). Four various distribution patterns of CNTs are considered in this study including the UD and three FG distributions of CNTs (FG-O, FG-X, and FG-V). The CNT volume fraction corresponding to these above four distribution patterns of reinforcement is given by[2–5]:

$$\text{UD CNTRC nanoplate: } V_{CNT} = V_{CNT}^{*} \tag{1}$$

$$\text{FG-O CNTRC nanoplate: } V_{CNT} = 2\left(1 - 2\frac{|z|}{h}\right)V_{CNT}^{*} \tag{2}$$

$$\text{FG-X CNTRC nanoplate: } V_{CNT} = 4\frac{|z|}{h}V_{CNT}^{*} \tag{3}$$

$$\text{FG-V CNTRC nanoplate: } V_{CNT} = \left(1 + 2\frac{z}{h}\right)V_{CNT}^{*} \tag{4}$$

where V_{CNT}^{*} is given CNT volume fraction which can be calculated as below[2–5]:

$$V_{CNT}^{*} = \frac{m_{CNT}}{m_{CNT} + (1 - m_{CNT})(\rho_{CNT}/\rho_{m})} \tag{5}$$

herein, m_{CNT} refers to the mass fraction of CNTs, while ρ_{m} and ρ_{CNT} are the mass densities of the polymer matrix and CNT, respectively. The extended rule of mixture proposed first by Shen[2–5] is employed to estimate the material properties of FG-CNTRC nanoplates including the Young's elastic moduli (E_{11} and E_{22}) and the shear elastic modulus (G_{12}) as below[2–5]:

$$E_{11} = \eta_{1} V_{CNT} E_{11}^{CNT} + V_{m} E^{m} \tag{6}$$

$$\frac{\eta_{2}}{E_{22}} = \frac{V_{CNT}}{E_{22}^{CNT}} + \frac{V_{m}}{E^{m}} \tag{7}$$

$$\frac{\eta_{3}}{G_{12}} = \frac{V_{CNT}}{G_{12}^{CNT}} + \frac{V_{m}}{G^{m}} \tag{8}$$

where E_{11}^{CNT}, E_{22}^{CNT} and G_{12}^{CNT} are denoted corresponding for the Young's elastic moduli and shear elastic modulus of CNT; E^{m} and G^{m} refer to the Young's elastic modulus and shear elastic modulus of the polymer matrix, respectively. The volume fraction of the polymer matrix is denoted by $V_{m} = 1 - V_{CNT}$. The size-dependent material properties of CNT are also captured by introducing the CNT efficiency parameters $\eta_{i}\,(i = 1,2,3)$. These CNT efficiency parameters depend on the chosen polymer matrix and can be determined by the MD simulation[2–5]. Also, the Poisson's ratio (ν_{12}) and the mass density (ρ) of the FG-CNTRC nanoplate can be determined by[2–5]:

$$\nu_{12} = V_{CNT}\nu_{12}^{CNT} + V_{m}\nu^{m} \tag{9}$$

$$\rho = V_{CNT}\rho^{CNT} + V_{m}\rho^{m} \tag{10}$$

where, ν_{12}^{CNT} and ν^{m} refer to the Poisson's ratios of CNT and polymer matrix, respectively.

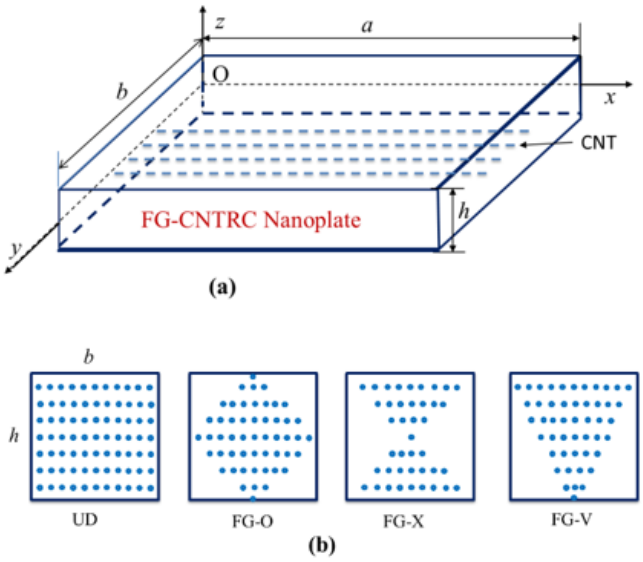

Figure 1. Configuration of an FG-CNTRC nanoplate **(a)**, and four different distribution patterns of CNTs **(b)**.

2.2. The nonlocal strain gradient theory

According to the NSGT proposed by Lim et al.[16], the total stress (t_{ij}) can be expressed as a function of the classical stress (σ_{ij}) and the higher-order stress ($\sigma_{ijm}^{(1)}$), as below:

$$t_{ij} = \sigma_{ij} - \nabla \sigma_{ijm}^{(1)} \tag{11}$$

where $\nabla = \partial/\partial x + \partial/\partial y$ is the differential operator; the classical and higher-order stresses are defined as [16]:

$$\sigma_{ij} = \int_V \alpha_0(\mathbf{x}', \mathbf{x}, e_0 a) C_{ijkl} \varepsilon'_{kl} dV' \tag{12}$$

$$\sigma_{ijm}^{(1)} = l^2 \int_V \alpha_1(\mathbf{x}', \mathbf{x}, e_1 a) C_{ijkl} \varepsilon'_{kl,m} dV' \tag{13}$$

in which, $\alpha_0(\mathbf{x}', \mathbf{x}, e_0 a)$ and $\alpha_1(\mathbf{x}', \mathbf{x}, e_1 a)$ are two kernel functions which are defined by Eringen[11,12]; $e_0 a$ and $e_1 a$ represent two nonlocal parameters used to evaluate the impact of the nonlocal stress effect; l is the material length scale parameter which is introduced to consider the impact of the strain gradient; C_{ijkl} are the elastic coefficients; while ε_{kl} and $\varepsilon_{kl,m}$ are respectively the strain and strain gradient components. The following conditions are assumed[16]:

$$\left[1 - (e_0 a)^2 \nabla^2\right] \sigma_{ij} = C_{ijkl} \varepsilon_{kl} \tag{14}$$

$$\left[1 - (e_1 a)^2 \nabla^2\right] \sigma_{ijm}^{(1)} = l^2 C_{ijkl} \varepsilon_{kl,m} \tag{15}$$

where $\nabla^2 = \partial^2/\partial x^2 + \partial^2/\partial y^2$ is the Laplacian operator. From Equations (11), (14), and (15), it can be derived the generalized constitutive equation[16]:

$$\left[1 - (e_1 a)^2 \nabla^2\right]\left[1 - (e_0 a)^2 \nabla^2\right] t_{ij} = \left[1 - (e_1 a)^2 \nabla^2\right] C_{ijkl} \varepsilon_{kl} - l^2 \left[1 - (e_0 a)^2 \nabla^2\right] C_{ijkl} \nabla^2 \varepsilon_{kl} \tag{16}$$

For simplicity, it can be assumed that $e_0 a = e_1 a = ea$. And therefore, the constitutive Equation (16) is simplified to:

$$\left[1 - (ea)^2 \nabla^2\right] t_{ij} = (1 - l^2 \nabla^2) C_{ijkl} \varepsilon_{kl} \tag{17}$$

2.3. The first-order shear deformation plate theory

According to the FSDPT, the displacement field (u_x, u_y, u_z) of the FG-CNTRC nanoplate can be represented as[6]:

$$u_x(x,y,z,t) = u(x,y,t) + z\varphi_x(x,y,t) \tag{18}$$

$$u_y(x,y,z,t) = v(x,y,t) + z\varphi_y(x,y,t) \tag{19}$$

$$u_z(x,y,z,t) = w(x,y,t) \tag{20}$$

where u, v and w are the mid-plane displacements of the FG-CNTRC nanoplate; φ_x and φ_y are denoted for the rotations; and t is time. Whereby, the strain components are:

$$\varepsilon_{xx} = \frac{\partial u}{\partial x} + z\frac{\partial \varphi_x}{\partial x}; \varepsilon_{yy} = \frac{\partial v}{\partial y} + z\frac{\partial \varphi_y}{\partial y} \tag{21a}$$

$$\gamma_{yz} = \frac{\partial w}{\partial y} + \varphi_y; \gamma_{zz} = \frac{\partial w}{\partial x} + \varphi_x; \gamma_{xy} = \frac{\partial u}{\partial y} + \frac{\partial v}{\partial x} + z\left(\frac{\partial \varphi_x}{\partial y} + \frac{\partial \varphi_y}{\partial x}\right). \tag{21b}$$

Employing Equation (17), the constitutive equations can be expressed as:

$$\left[1-(ea)^2\nabla^2\right]\begin{Bmatrix} t_{xx} \\ t_{yy} \\ t_{yz} \\ t_{xz} \\ t_{xy} \end{Bmatrix} = \left(1-l^2\nabla^2\right)\begin{bmatrix} Q_{11} & Q_{12} & 0 & 0 & 0 \\ Q_{12} & Q_{22} & 0 & 0 & 0 \\ 0 & 0 & Q_{44} & 0 & 0 \\ 0 & 0 & 0 & Q_{55} & 0 \\ 0 & 0 & 0 & 0 & Q_{66} \end{bmatrix}\begin{Bmatrix} \varepsilon_{xx} \\ \varepsilon_{yy} \\ \gamma_{yz} \\ \gamma_{xz} \\ \gamma_{xy} \end{Bmatrix} \tag{22}$$

where

$$Q_{11} = \frac{E_{11}}{1-\nu_{12}\nu_{21}}, Q_{22} = \frac{E_{22}}{1-\nu_{12}\nu_{21}}, Q_{12} = \frac{\nu_{12}E_{22}}{1-\nu_{12}\nu_{21}}, Q_{44} = G_{23}, Q_{55} = G_{13}, Q_{66} = G_{12} \tag{23}$$

The virtual strain energy of the FG-CNTRC nanoplate takes the following form:

$$\begin{aligned} \delta U &= \int_A \int_{-h/2}^{h/2} t_{ij}\delta\varepsilon_{ij} dz dA \\ &= \int_A \begin{bmatrix} N_{xx}\frac{\partial \delta u}{\partial x} + N_{yy}\frac{\partial \delta v}{\partial y} + N_{xy}\left(\frac{\partial \delta u}{\partial y} + \frac{\partial \delta v}{\partial x}\right) + M_{xx}\frac{\partial \delta \varphi_x}{\partial x} + M_{yy}\frac{\partial \delta \varphi_y}{\partial y} \\ +M_{xy}\left(\frac{\partial \delta \varphi_y}{\partial x} + \frac{\partial \delta \varphi_x}{\partial y}\right) + Q_x\left(\frac{\partial \delta w}{\partial x} + \delta\varphi_x\right) + Q_y\left(\frac{\partial \delta w}{\partial y} + \delta\varphi_y\right) \end{bmatrix} dA \end{aligned} \tag{24}$$

where, N_{xx}, N_{yy} and N_{xy} represent the normal and shearing forces; M_{xx}, M_{yy} and M_{xy} are denoted for the bending moments; Q_x and Q_y are transverse shearing force intensities; which are defined as:

$$\left(N_{xx}, N_{yy}, N_{xy}\right) = \int_{-h/2}^{h/2} \left(t_{xx}, t_{yy}, t_{xy}\right) dz \tag{25}$$

$$\left(M_{xx}, M_{yy}, M_{xy}\right) = \int_{-h/2}^{h/2} \left(t_{xx}, t_{yy}, t_{xy}\right) z dz \tag{26}$$

$$\left(Q_x, Q_y\right) = k_s \int_{-h/2}^{h/2} \left(t_{xz}, t_{yz}\right) dz \tag{27}$$

herein, $k_s = 5/6$ is the shear correction factor. The virtual kinetic energy of the FG-CNTRC nanoplate can be determined as:

$$\delta K = \int_A \left\{ \int_{-h/2}^{h/2} \begin{bmatrix} I_0(\dot{u}\delta\dot{u} + \dot{v}\delta\dot{v} + \dot{w}\delta\dot{w}) + I_1(\dot{\varphi}_x\delta\dot{u} + \dot{u}\delta\dot{\varphi}_x + \dot{\varphi}_y\delta\dot{v} + \dot{v}\delta\dot{\varphi}_y) \\ + I_2(\dot{\varphi}_x\delta\dot{\varphi}_x + \dot{\varphi}_y\delta\dot{\varphi}_y) \end{bmatrix} \right\} dA \tag{28}$$

in which, I_0, I_1 and I_2 are the mass moments of inertia which are defined as:

$$\left(I_0, I_1, I_2\right) = \int_{-h/2}^{h/2} \rho\left(1, z, z^2\right) dz \tag{29}$$

The virtual work done by the applied mechanical load $q(x,y,t)$ is:

$$\delta V = \int_A q\delta w dA \tag{30}$$

The governing equations of motion can be derived by applying the Hamilton's principle:

$$\int_0^T \left(\delta U + \delta V - \delta K\right) dt = 0 \tag{31}$$

Substituting Equations (24), (28) and (30) into Equation (31), the governing equations of motion can be obtained as:

$$\frac{\partial N_{xx}}{\partial x} + \frac{\partial N_{xy}}{\partial y} = I_0\ddot{u} + I_1\ddot{\varphi}_x \tag{32}$$

$$\frac{\partial N_{xy}}{\partial x} + \frac{\partial N_{yy}}{\partial y} = I_0\ddot{v} + I_1\ddot{\varphi}_y \tag{33}$$

$$\frac{\partial M_{xx}}{\partial x} + \frac{\partial M_{xy}}{\partial y} - Q_x = I_2\ddot{\varphi}_x + I_1\ddot{u} \tag{34}$$

$$\frac{\partial M_{xy}}{\partial x} + \frac{\partial M_{yy}}{\partial y} - Q_y = I_2\ddot{\varphi}_y + I_1\ddot{v} \tag{35}$$

$$\frac{\partial Q_x}{\partial x} + \frac{\partial Q_y}{\partial y} + q = I_0\ddot{w} \tag{36}$$

Putting Equation (22) into Equations (25)–(28), it can be obtained:

$$\left[1-(ea)^2\nabla^2\right] N_{xx} = \left(1-l^2\nabla^2\right)\left[A_{11}\frac{\partial u}{\partial x} + B_{11}\frac{\partial \varphi_x}{\partial x} + A_{12}\frac{\partial v}{\partial y} + B_{12}\frac{\partial \varphi_y}{\partial y} \right] \tag{37a}$$

$$\left[1-(ea)^2\nabla^2\right] N_{yy} = \left(1-l^2\nabla^2\right)\left[A_{12}\frac{\partial u}{\partial x} + B_{12}\frac{\partial \varphi_x}{\partial x} + A_{22}\frac{\partial v}{\partial y} + B_{22}\frac{\partial \varphi_y}{\partial y} \right] \tag{37b}$$

$$\left[1-(ea)^2\nabla^2\right] N_{xy} = \left(1-l^2\nabla^2\right)\left[A_{66}\left(\frac{\partial u}{\partial y} + \frac{\partial v}{\partial x}\right) + B_{66}\left(\frac{\partial \varphi_x}{\partial y} + \frac{\partial \varphi_y}{\partial x}\right) \right] \tag{37c}$$

$$\left[1-(ea)^2\nabla^2\right]M_{xx}=\left(1-l^2\nabla^2\right)\left[B_{11}\frac{\partial u}{\partial x}+D_{11}\frac{\partial \varphi_x}{\partial x}+B_{12}\frac{\partial v}{\partial y}+D_{12}\frac{\partial \varphi_y}{\partial y}\right] \tag{37d}$$

$$\left[1-(ea)^2\nabla^2\right]M_{yy}=\left(1-l^2\nabla^2\right)\left[B_{11}\frac{\partial u}{\partial x}+D_{11}\frac{\partial \varphi_x}{\partial x}+B_{12}\frac{\partial v}{\partial y}+D_{12}\frac{\partial \varphi_y}{\partial y}\right] \tag{37e}$$

$$\left[1-(ea)^2\nabla^2\right]M_{xy}=\left(1-l^2\nabla^2\right)\left[B_{66}\left(\frac{\partial u}{\partial y}+\frac{\partial v}{\partial x}\right)+D_{66}\left(\frac{\partial \varphi_x}{\partial y}+\frac{\partial \varphi_y}{\partial x}\right)\right] \tag{37f}$$

$$\left[1-(ea)^2\nabla^2\right]Q_x=\left(1-l^2\nabla^2\right)\left[k_sA_{44}\left(\frac{\partial w}{\partial x}+\varphi_x\right)\right] \tag{37g}$$

$$\left[1-(ea)^2\nabla^2\right]Q_y=\left(1-l^2\nabla^2\right)\left[k_sA_{55}\left(\frac{\partial w}{\partial y}+\varphi_y\right)\right] \tag{37h}$$

where

$$\left(A_{11},B_{11},D_{11}\right)=\int_{-h/2}^{h/2}Q_{11}\left(1,z,z^2\right)dz \tag{38a}$$

$$\left(A_{12},B_{12},D_{12}\right)=\int_{-h/2}^{h/2}Q_{12}\left(1,z,z^2\right)dz \tag{38b}$$

$$\left(A_{22},B_{22},D_{22}\right)=\int_{-h/2}^{h/2}Q_{22}\left(1,z,z^2\right)dz \tag{38c}$$

$$\left(A_{66},B_{66},D_{66}\right)=\int_{-h/2}^{h/2}Q_{66}\left(1,z,z^2\right)dz \tag{38d}$$

$$\left(A_{44},A_{55}\right)=\int_{-h/2}^{h/2}\left(Q_{44},Q_{55}\right)dz \tag{38e}$$

The governing equations of motion in terms of displacements can be obtained by substituting Equation (38) into Equations (32)–(36) as below:

$$\begin{aligned}&\left(1-l^2\nabla^2\right)\left\{\begin{array}{l}A_{11}\dfrac{\partial^2u}{\partial x^2}+A_{12}\dfrac{\partial^2v}{\partial x\partial y}+A_{66}\left(\dfrac{\partial^2v}{\partial x\partial y}+\dfrac{\partial^2u}{\partial y^2}\right)\\+B_{11}\dfrac{\partial^2\varphi_x}{\partial x^2}+B_{12}\dfrac{\partial^2\varphi_y}{\partial x\partial y}+B_{66}\left(\dfrac{\partial^2\varphi_y}{\partial x\partial y}+\dfrac{\partial^2\varphi_x}{\partial y^2}\right)\end{array}\right\}\\&=\left[1-(ea)^2\nabla^2\right]\left(I_0\frac{\partial^2u}{\partial t^2}+I_1\frac{\partial^2\varphi_x}{\partial t^2}\right)\end{aligned} \tag{39}$$

$$\begin{aligned}&\left(1-l^2\nabla^2\right)\left\{\begin{array}{l}A_{12}\dfrac{\partial^2u}{\partial x\partial y}+A_{22}\dfrac{\partial^2v}{\partial y^2}+A_{66}\left(\dfrac{\partial^2u}{\partial x\partial y}+\dfrac{\partial^2v}{\partial x^2}\right)\\+B_{22}\dfrac{\partial^2\varphi_y}{\partial y^2}+B_{12}\dfrac{\partial^2\varphi_x}{\partial x\partial y}+B_{66}\left(\dfrac{\partial^2\varphi_x}{\partial x\partial y}+\dfrac{\partial^2\varphi_y}{\partial x^2}\right)\end{array}\right\}\\&=\left[1-(ea)^2\nabla^2\right]\left(I_0\frac{\partial^2v}{\partial t^2}+I_1\frac{\partial^2\varphi_y}{\partial t^2}\right)\end{aligned} \tag{40}$$

$$\left(1-l^2\nabla^2\right)\left\{\begin{array}{l} B_{11}\dfrac{\partial^2 u}{\partial x^2}+B_{12}\dfrac{\partial^2 v}{\partial x\partial y}+D_{11}\dfrac{\partial^2 \varphi_x}{\partial x^2}+D_{12}\dfrac{\partial^2 \varphi_y}{\partial x\partial y} \\ +B_{66}\left(\dfrac{\partial^2 v}{\partial x\partial y}+\dfrac{\partial^2 u}{\partial y^2}\right)+D_{66}\left(\dfrac{\partial^2 \varphi_y}{\partial x\partial y}+\dfrac{\partial^2 \varphi_x}{\partial y^2}\right)-k_s A_{44}\left(\dfrac{\partial w}{\partial x}+\varphi_x\right) \end{array}\right\} \tag{41}$$
$$=\left[1-(ea)^2\nabla^2\right]\left(I_2\frac{\partial^2 \varphi_x}{\partial t^2}+I_1\frac{\partial^2 u}{\partial t^2}\right)$$

$$\left(1-l^2\nabla^2\right)\left\{\begin{array}{l} B_{12}\dfrac{\partial^2 u}{\partial x\partial y}+B_{22}\dfrac{\partial^2 v}{\partial y^2}+D_{12}\dfrac{\partial^2 \varphi_x}{\partial x\partial y}+D_{22}\dfrac{\partial^2 \varphi_y}{\partial y^2} \\ +B_{66}\left(\dfrac{\partial^2 v}{\partial x^2}+\dfrac{\partial^2 u}{\partial x\partial y}\right)+D_{66}\left(\dfrac{\partial^2 \varphi_y}{\partial x^2}+\dfrac{\partial^2 \varphi_x}{\partial x\partial y}\right)-k_s A_{55}\left(\dfrac{\partial w}{\partial y}+\varphi_y\right) \end{array}\right\} \tag{42}$$
$$=\left[1-(ea)^2\nabla^2\right]\left(I_2\frac{\partial^2 \varphi_y}{\partial t^2}+I_1\frac{\partial^2 v}{\partial t^2}\right)$$

$$\begin{array}{l} \left(1-l^2\nabla^2\right)\left\{k_s A_{44}\left(\dfrac{\partial^2 w}{\partial x^2}+\dfrac{\partial \varphi_x}{\partial x}\right)+k_s A_{55}\left(\dfrac{\partial^2 w}{\partial y^2}+\dfrac{\partial \varphi_y}{\partial y}\right)+q(x,y,t)\right\} \\ =\left[1-(ea)^2\nabla^2\right]\left(I_0\dfrac{\partial^2 w}{\partial t^2}\right) \end{array} \tag{43}$$

3. Solution procedure

In this study, the rectangular FG-CNTRC nanoplate with simply-supported both edges is considered. The mathematical representation of this boundary conditions is as follows:

$$\begin{array}{l} w=\varphi_x=M_{xx}=0 \text{ at } x=0 \text{ and } x=a \\ w=\varphi_y=M_{yy}=0 \text{ at } y=0 \text{ and } y=b \end{array} \tag{44}$$

The displacement components are chosen as follows:

$$u=\sum_{m=1}^{\infty}\sum_{n=1}^{\infty}U_{mn}e^{i\omega t}\cos(\alpha x)\sin(\beta y) \tag{45}$$

$$v=\sum_{m=1}^{\infty}\sum_{n=1}^{\infty}V_{mn}e^{i\omega t}\sin(\alpha x)\cos(\beta y) \tag{46}$$

$$\varphi_x=\sum_{m=1}^{\infty}\sum_{n=1}^{\infty}X_{mn}e^{i\omega t}\cos(\alpha x)\sin(\beta y) \tag{47}$$

$$\varphi_y=\sum_{m=1}^{\infty}\sum_{n=1}^{\infty}Y_{mn}e^{i\omega t}\sin(\alpha x)\cos(\beta y) \tag{48}$$

$$w=\sum_{m=1}^{\infty}\sum_{n=1}^{\infty}W_{mn}e^{i\omega t}\sin(\alpha x)\sin(\beta y) \tag{49}$$

where U_{mn}, V_{mn}, X_{mn}, Y_{mn} and W_{mn} are unknown coefficients, ω is the natural frequency of the FG-CNTRC nanoplate, $i=\sqrt{-1}$, $\alpha=m\pi/a$ and $\beta=n\pi/b$. For the vibration problem, the applied mechanical load *q(x,y,t)* in the governing equations of motion is omitted. Substituting the above solutions given in Equations (45)–(49) into the governing Equations of motion (39)–(43), it can be obtained:

$$\left[\begin{pmatrix} s_{11} & s_{12} & s_{13} & s_{14} & s_{15} \\ s_{21} & s_{22} & s_{23} & s_{24} & s_{25} \\ s_{31} & s_{32} & s_{33} & s_{34} & s_{35} \\ s_{41} & s_{42} & s_{43} & s_{44} & s_{45} \\ s_{51} & s_{52} & s_{53} & s_{54} & s_{55} \end{pmatrix} - \omega^2 \begin{pmatrix} m_{11} & m_{12} & m_{13} & m_{14} & m_{15} \\ m_{21} & m_{22} & m_{23} & m_{24} & m_{25} \\ m_{31} & m_{32} & m_{33} & m_{34} & m_{35} \\ m_{41} & m_{42} & m_{43} & m_{44} & m_{45} \\ m_{51} & m_{52} & m_{53} & m_{54} & m_{55} \end{pmatrix}\right] \begin{pmatrix} U_{mn} \\ V_{mn} \\ X_{mn} \\ Y_{mn} \\ W_{mn} \end{pmatrix} = \begin{pmatrix} 0 \\ 0 \\ 0 \\ 0 \\ 0 \end{pmatrix} \tag{50}$$

where

$$\begin{gathered}
s_{11} = A_{11}\left[\alpha^2 + l^2(\alpha^4 + \alpha^2\beta^2)\right] + A_{66}\left[\beta^2 + l^2(\alpha^2\beta^2 + \beta^4)\right], \\
s_{12} = A_{12}\left[\alpha\beta + l^2(\alpha^3\beta + \alpha\beta^3)\right] + A_{66}\left[\alpha\beta + l^2(\alpha^3\beta + \alpha\beta^3)\right], \\
s_{13} = B_{11}\left[\alpha^2 + l^2(\alpha^4 + \alpha^2\beta^2)\right] + B_{66}\left[\beta^2 + l^2(\alpha^2\beta^2 + \beta^4)\right], \\
s_{14} = B_{12}\left[\alpha\beta + l^2(\alpha^3\beta + \alpha\beta^3)\right] + B_{66}\left[\alpha\beta + l^2(\alpha^3\beta + \alpha\beta^3)\right], \\
s_{21} = A_{12}\left[\alpha\beta + l^2(\alpha^3\beta + \alpha\beta^3)\right] + A_{66}\left[\alpha\beta + l^2(\alpha^3\beta + \alpha\beta^3)\right], \\
s_{22} = A_{22}\left[\beta^2 + l^2(\alpha^2\beta^2 + \beta^4)\right] + A_{66}\left[\alpha\beta + l^2(\alpha^4 + \alpha^2\beta^2)\right], \\
s_{23} = B_{12}\left[\alpha\beta + l^2(\alpha^3\beta + \alpha\beta^3)\right] + B_{66}\left[\alpha\beta + l^2(\alpha^3\beta + \alpha\beta^3)\right], \\
s_{24} = B_{12}\left[\beta^2 + l^2(\alpha^2\beta^2 + \beta^4)\right] + B_{66}\left[\alpha^2 + l^2(\alpha^4 + \alpha^2\beta^2)\right], \\
s_{31} = B_{11}\left[\alpha^2 + l^2(\alpha^4 + \alpha^2\beta^2)\right] + B_{66}\left[\beta^2 + l^2(\alpha^2\beta^2 + \beta^4)\right] \\
s_{32} = B_{12}\left[\alpha\beta + l^2(\alpha^3\beta + \alpha\beta^3)\right] + B_{66}\left[\alpha\beta + l^2(\alpha^3\beta + \alpha\beta^3)\right] \\
s_{33} = D_{11}\left[\alpha^2 + l^2(\alpha^4 + \alpha^2\beta^2)\right] + D_{66}\left[\beta^2 + l^2(\alpha^2\beta^2 + \beta^4)\right] + k_s A_{44}\left[1 + l^2(\alpha^2 + \beta^2)\right] \\
s_{34} = D_{12}\left[\alpha\beta + l^2(\alpha^3\beta + \alpha\beta^3)\right] + D_{66}\left[\left[\alpha\beta + l^2(\alpha^3\beta + \alpha\beta^3)\right]\right] \\
s_{35} = k_s A_{55}\left[\alpha + l^2(\alpha^3 + \alpha\beta^2)\right] \; s_{41} = B_{12}\left[\alpha\beta + l^2(\alpha^3\beta + \alpha\beta^3)\right] + B_{66}\left[\alpha\beta + l^2(\alpha^3\beta + \alpha\beta^3)\right] \\
s_{42} = B_{22}\left[\beta^2 + l^2(\alpha^2\beta^2 + \beta^4)\right] + B_{66}\left[\alpha^2 + l^2(\alpha^4 + \alpha^2\beta^2)\right] \\
s_{43} = D_{12}\left[\alpha\beta + l^2(\alpha^3\beta + \alpha\beta^3)\right] + D_{66}\left[\alpha\beta + l^2(\alpha^3\beta + \alpha\beta^3)\right] \\
s_{44} = D_{22}\left[\beta^2 + l^2(\alpha^2\beta^2 + \beta^4)\right] + D_{66}\left[\alpha^2 + l^2(\alpha^4 + \alpha^2\beta^2)\right] + k_s A_{55}\left[1 + l^2(\alpha^2 + \beta^2)\right] \\
s_{45} = k_s A_{44}\left[\beta + l^2(\alpha^2\beta + \beta^3)\right] \\
s_{53} = k_s A_{55}\left[\alpha + l^2(\alpha^3 + \alpha\beta^2)\right] \; s_{54} = k_s A_{44}\left[\beta + l^2(\alpha^2\beta + \beta^3)\right] \\
s_{55} = k_s A_{44}\left[\alpha^2 + l^2(\alpha^4 + \alpha^2\beta^2)\right] + k_s A_{55}\left[\beta^2 + l^2(\alpha^2\beta^2 + \beta^4)\right] \\
s_{15} = s_{25} = s_{51} = s_{52} = 0.
\end{gathered} \tag{51}$$

$$\begin{gathered}
m_{11} = I_0\left[1 + (ea)^2(\alpha^2 + \beta^2)\right], \quad m_{12} = I_1\left[1 + (ea)^2(\alpha^2 + \beta^2)\right], \\
m_{22} = I_0\left[1 + (ea)^2(\alpha^2 + \beta^2)\right], \quad m_{24} = I_1\left[1 + (ea)^2(\alpha^2 + \beta^2)\right], \\
m_{31} = I_1\left[1 + (ea)^2(\alpha^2 + \beta^2)\right], \quad m_{33} = I_2\left[1 + (ea)^2(\alpha^2 + \beta^2)\right] \\
m_{42} = I_1\left[1 + (ea)^2(\alpha^2 + \beta^2)\right], \quad m_{44} = I_2\left[1 + (ea)^2(\alpha^2 + \beta^2)\right] \; m_{55} = I_0\left[1 + (ea)^2(\alpha^2 + \beta^2)\right], \\
m_{13} = m_{14} = m_{15} = m_{21} = m_{23} = m_{25} = 0, \\
m_{32} = m_{34} = m_{35} = m_{41} = m_{43} = m_{45} = m_{51} = m_{52} = m_{53} = m_{54} = 0.
\end{gathered} \tag{52}$$

4. Numerical results and discussions

In this section, numerical illustrations are performed to verify the reliability of the obtained results as well as estimate the influence of some key parameters on the free vibration response of FG-CNTRC nanoplates. For this purpose, Poly{(m-phenylenevinylene)-co-[(2,5-dioctoxy-p-phenylene) vinylene]}, referred to as PmPV, is considered as the polymer matrix, the material properties of the polymer matrix are [2]: $E^m = 2.1\text{GPa}$, $\rho^m = 1150\text{kg/m}^3$, and $\nu^m = 0.34$ at room temperature (T = 300 K). The armchair (10,10) single-walled CNTs are selected as the reinforcements which have the material properties[2]: $E_{11}^{CNT} = 5.6466\text{TPa}$, $E_{22}^{CNT} = 7.0800\text{TPa}$, $G_{12}^{CNT} = 1.9445\text{TPa}$, $\rho^{CNT} = 1400\text{kg/m}^3$, and $\nu_{12}^{CNT} = 0.175$. The CNT efficiency parameters $\eta_i\,(i = 1, 2, 3)$ for some given CNTs volume fractions V_{CNT}^* can be estimated by the MD simulation and given in **Table 1**.

Table 1. The CNTs efficiency parameters[2].

V_{CNT}^*	η_1	η_2	η_3
0.11	0.149	0.934	0.934
0.14	0.150	0.941	0.941
0.17	0.149	1.381	1.381

The dimensionless frequency is defined:

$$\Omega = \omega \frac{a^2}{h}\sqrt{\frac{\rho^m}{E^m}} \tag{53}$$

4.1. Validation study

The dimensionless frequencies obtained in this work and those of Zhu et al.[6] for FG-CNTRC square plates are compared and presented in **Table 2** for some values of the CNT volume fraction (V_{CNT}^*) and the length-to-thickness ratio (a/h). It is noted that the results for FG-CNTRC plates based on the CET can be derived from the present results for FG-CNTRC nanoplates based on the NSGT by letting the nonlocal and material length scale parameters equal to zero ($ea = l = 0$). The results of Zhu et al.[6] were carried out by employing the finite element method. It is possible to observe the accuracy of the obtained analytical results compared with the numerical results of Zhu et al.[6].

Table 2. Comparison of the dimensionless frequencies (Ω) of FG-CNTRC square plates, (m = 1, n = 1).

V_{CNT}^*	a/h	UD		FG-O		FG-X		FG-V	
		Present	Ref. [6]	Present	Ref. [6]	Present	Ref. [6]	Present	Ref. [6]
0.11	10	13.506	13.532	11.526	11.550	14.591	14.616	12.425	12.452
	20	17.303	17.355	13.484	13.523	19.880	19.939	15.063	15.110
	50	19.153	19.223	14.257	14.302	22.896	22.984	16.193	16.252
0.14	10	14.294	14.306	12.329	12.338	15.356	15.368	13.243	13.256
	20	18.893	18.921	14.765	14.784	21.611	21.642	16.485	16.510
	50	21.315	21.354	15.778	15.801	25.505	25.555	17.962	17.995
0.17	10	16.780	16.815	14.254	14.282	18.241	18.278	15.427	15.461
	20	21.387	21.456	16.582	16.628	24.683	24.764	18.577	18.638
	50	23.605	23.697	17.489	17.544	28.295	28.413	19.908	19.982

4.2. Parametric study

The dimensionless frequencies (Ω) of FG-CNTRC nanoplates based on the NSGT for some different values of the CNT volume fraction (V_{CNT}^{*}), the length-to-thickness ratio (a/h) and distribution patterns of CNTs are listed in **Table 3**. The thickness of the nanoplate is considered as $h=10\,\text{nm}$, and the nonlocal and material length scale parameters are assumed as $ea=2\,\text{nm}$ and $l=1\,\text{nm}$. It can be observed that the dimensionless frequencies of FG-CNTRC nanoplates increase when increasing the length-to-thickness ratio (a/h) especially for small values of the length-to-thickness ratio. The dimensionless frequencies of FG-CNTRC nanoplates does not change much with large values of the length-to-thickness ratio. The CNT volume fraction (V_{CNT}^{*}) has an important impact on the free vibration behavior of FG-CNTRC nanoplates. As can be observed that the dimensionless frequencies of FG-CNTRC nanoplates increases sharply when increasing the CNT volume fraction. Furthermore, **Table 3** also reveals that among the FG-CNTRC nanoplates, the FG-X nanoplate has the maximum frequency and the FG-O nanoplate has the minimum frequency. For case of $a/h=5$, the frequencies of FG-CNTRC nanoplates increase about 3-4% when the CNT volume fraction increases from $V_{CNT}^{*}=0.11$ to $V_{CNT}^{*}=0.14$. The effect of the length-to-thickness ratio (a/h) and the distribution patterns of CNTs on the linear vibration behavior of FG-CNTRC nanoplates can be also observed in **Figure 2** for some different values of the CNT volume fraction (V_{CNT}^{*}).

Table 3. Dimensionless frequencies (Ω) of FG-CNTRC square nanoplates.

V_{CNT}^{*}	a/h	Mode (m,n)	UD	FG-O	FG-X	FG-V
0.11	5	(1,1)	8.522	8.031	8.770	8.295
		(2,2)	19.059	18.787	19.302	19.018
		(3,3)	29.329	29.131	29.631	29.385
	10	(1,1)	13.467	11.492	14.548	12.389
		(2,2)	34.090	32.124	35.082	33.183
		(3,3)	55.108	53.670	56.023	54.625
	20	(1,1)	17.290	13.474	19.866	15.052
		(2,2)	53.868	45.971	58.194	49.556
		(3,3)	94.750	86.096	99.064	90.374
	50	(1,1)	19.151	14.255	22.893	16.191
		(2,2)	72.068	55.170	84.022	62.035
		(3,3)	148.630	118.043	168.312	130.922
0.14	5	(1,1)	8.781	8.335	9.032	8.594
		(2,2)	19.439	19.185	19.751	19.451
		(3,3)	29.868	29.868	30.291	29.990
	10	(1,1)	14.252	12.292	15.311	13.204
		(2,2)	35.126	33.343	36.131	34.377
		(3,3)	56.354	55.064	57.411	56.061
	20	(1,1)	18.879	14.754	21.595	16.472
		(2,2)	57.008	49.171	61.244	52.819
		(3,3)	98.517	90.414	102.714	94.603

Table 3. (*Continued*).

V^*_{CNT}	a/h	Mode (m,n)	UD	FG-O	FG-X	FG-V
	50	(1,1)	21.312	15.776	25.502	17.960
		(2,2)	79.253	60.6673	92.131	68.247
		(3,3)	161.134	128.661	181.478	142.491
0.17	5	(1,1)	10.637	10.002	11.029	10.380
		(2,2)	23.835	23.471	24.354	23.890
		(3,3)	36.937	37.401	36.419	36.691
	10	(1,1)	16.730	14.212	18.187	15.381
		(2,2)	42.550	40.008	44.118	41.520
		(3,3)	68.881	67.002	70.613	68.541
	20	(1,1)	21.371	16.570	24.664	18.564
		(2,2)	66.923	56.848	72.750	61.526
		(3,3)	118.072	106.936	124.313	112.750
	50	(1,1)	23.602	17.486	28.292	19.905
		(2,2)	88.981	67.777	104.142	76.413
		(3,3)	183.921	145.317	209.314	161.689

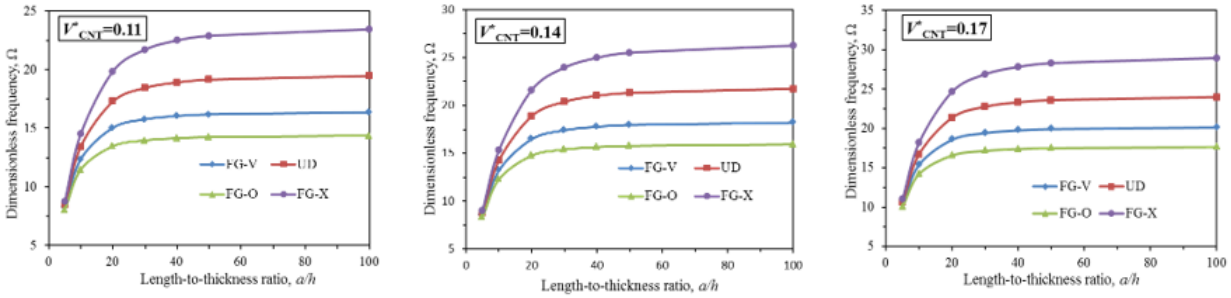

Figure 2. Variation of the dimensionless frequencies (Ω) to the length-to-thickness ratio (a/h), (m = 1, n = 1), ea = 2 nm, l = 1 nm.

The dimensionless frequencies of FG-CNTRC nanoplates for some values of the nonlocal parameter (ea) and the material length scale parameter (l) are showed in **Table 4**. As can see from **Table 4** that the dimensionless frequencies of FG-CNTRC nanoplates increasing as increasing the material length scale parameter (l) or by reducing the nonlocal parameter (ea). Also, **Table 4** reveals that the dimensionless frequencies of FG-CNTRC nanoplates based on the NSGT are always equal to the dimensionless frequencies of classical FG-CNTRC nanoplates (ea = l = 0) when the nonlocal parameter equals to the material length scale parameter (ea = l). The influence of the size-dependence on the vibration behavior of FG-CNTRC nanoplates can be observed in **Figure 3**. It can be seen that the results for the NSGT are equal to those for the CET when the scale ratio (l/ea) equals to 1(i.e., $ea = l$). When the scale ratio is larger than 1(i.e., $l > ea$), the frequencies of FG-CNTRC nanoplates increase by increasing the nonlocal parameter (ea), it means that the FG-CNTRC nanoplates arise the hardening-stiffness effect. On the other hand, when the scale ratio is smaller than 1(i.e., $l < ea$), the frequencies of FG-CNTRC nanoplates reduce as increasing the nonlocal parameter (ea), it means that the FG-CNTRC nanoplates arise the softening-stiffness effect.

Table 4. Dimensionless frequencies (Ω) of FG-CNTRC nanoplates, a/h = 15.

ea (nm)	Type	V^*_{CNT} = 0.11			V^*_{CNT} = 0.14			V^*_{CNT} = 0.17		
		l=0 (nm)	*l*=1 (nm)	*l*=2 (nm)	*l*=0 (nm)	*l*=1 (nm)	*l*=2 (nm)	*l*=0 (nm)	*l*=1 (nm)	*l*=2 (nm)
Mode (1,1)										
0	UD	**16.007**	16.014	16.035	**17.274**	17.282	17.304	**19.823**	19.832	19.858
	FG-O	**12.876**	12.882	12.899	**13.990**	13.996	14.014	**15.863**	15.870	15.891
	FG-X	**17.960**	17.968	17.992	**19.268**	19.277	19.302	**22.359**	22.369	22.398
	FG-V	**14.211**	14.218	14.236	**15.410**	15.417	15.437	**17.567**	17.575	17.598
1	UD	16.000	**16.007**	16.028	17.266	**17.274**	17.297	19.814	**19.823**	19.849
	FG-O	12.871	**12.876**	12.893	13.984	**13.990**	14.008	15.856	**15.863**	15.884
	FG-X	17.953	**17.960**	17.984	19.260	**19.268**	19.293	22.349	**22.359**	22.388
	FG-V	14.205	**14.211**	14.230	15.403	**15.410**	15.430	17.560	**17.567**	17.590
2	UD	15.979	15.986	**16.007**	17.244	17.251	**17.274**	19.788	19.797	**19.823**
	FG-O	12.854	12.859	**12.876**	13.965	13.972	**13.990**	15.836	15.843	**15.863**
	FG-X	17.929	17.937	**17.960**	19.234	19.243	**19.268**	22.320	22.330	**22.359**
	FG-V	14.187	14.193	**14.211**	15.383	15.390	**15.410**	17.537	17.544	**17.567**
Mode (3,3)										
0	UD	**77.599**	77.905	78.815	**79.957**	80.272	81.210	**96.857**	97.239	98.375
	FG-O	**73.124**	73.412	74.270	**75.899**	76.198	77.089	**91.071**	91.429	92.497
	FG-X	**79.857**	80.171	81.108	**82.244**	82.568	83.533	**100.425**	100.821	101.999
	FG-V	**75.534**	75.832	76.718	**78.252**	78.560	79.478	**94.512**	94.884	95.992
1	UD	77.295	**77.599**	78.506	79.643	**79.957**	80.891	96.477	**96.857**	97.988
	FG-O	72.837	**73.124**	73.978	75.601	**75.899**	76.786	90.713	**91.071**	92.134
	FG-X	79.543	**79.857**	80.789	81.921	**82.244**	83.205	100.031	**100.425**	101.599
	FG-V	75.238	**75.534**	76.417	77.945	**78.252**	79.166	94.141	**94.5120**	95.616
2	UD	76.402	76.703	**77.599**	78.723	79.033	**79.957**	95.363	95.738	**96.857**
	FG-O	71.996	72.280	**73.124**	74.728	75.023	**75.899**	89.666	90.019	**91.071**
	FG-X	78.625	78.934	**79.857**	80.975	81.294	**82.244**	98.876	99.266	**100.425**
	FG-V	74.369	74.662	**75.534**	77.045	77.348	**78.252**	93.054	93.420	**94.512**

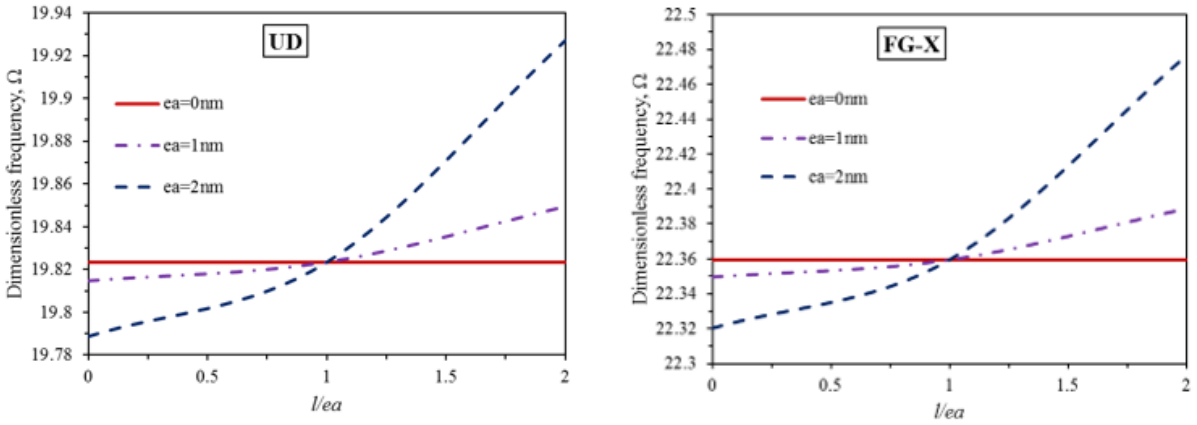

Figure 3. Variation of the dimensionless frequencies (Ω) to the scale ratio (l/ea), (m = 1, n = 1), $a = 15h$, $V^*_{CNT} = 0.11$.

Table 5 lists the dimensionless frequencies of FG-CNTRC nanoplates for some values of the CNT volume fraction (V^*_{CNT}) and the width-to-length ratio (b/a). It can be observed that the dimensionless

frequencies of FG-CNTRC nanoplates reduce as increasing the width-to-length ratio (b/a). It means that when increasing the width-to-length ratio (b/a), the stiffness of FG-CNTRC nanoplates reduces. For the fundamental vibration mode (m = 1, n = 1) and in case of $V_{CNT}^{*} = 0.11$, it can be estimated that the frequencies of FG-X nanoplates with b/a = 2 reduce about 2.2% compared with the frequencies of FG-X square nanoplates; and the frequencies of FG-O nanoplates with b/a = 2 decrease about 5% compared with the frequencies of FG-O square nanoplates.

Table 5. Dimensionless frequencies (Ω) of FG-CNTRC nanoplates, a = 20 h, ea = 1 nm, l = 2 nm.

V_{CNT}^{*}	b/a	Mode (1,1)				Mode (3,3)			
		UD	FG-O	FG-X	FG-V	UD	FG-O	FG-X	FG-V
0.11	0.5	21.436	18.414	23.701	19.826	134.483	128.426	138.762	132.546
	1	17.316	13.494	19.895	15.074	96.007	87.238	100.379	91.573
	1.5	16.905	12.953	19.535	14.568	92.183	82.685	96.715	87.209
	2	16.794	12.802	19.440	14.429	91.265	81.510	95.868	86.109
0.14	0.5	22.820	19.414	25.316	21.042	138.040	131.734	142.984	136.489
	1	18.907	14.776	21.627	16.497	99.823	91.613	104.077	95.858
	1.5	18.529	14.283	21.289	16.029	96.140	87.366	100.435	91.685
	2	18.428	14.147	21.201	15.902	95.276	86.296	99.608	90.660
0.17	0.5	26.607	22.659	29.706	24.659	167.957	159.170	175.628	166.252
	1	21.403	16.594	24.701	18.591	119.639	108.355	125.962	114.245
	1.5	20.883	15.928	24.225	17.945	114.819	102.752	121.155	108.678
	2	20.742	15.742	24.099	17.767	113.660	101.305	120.037	107.276

5. Conclusion

Analytical solutions for the free vibration problem of FG-CNTRC nanoplates with simply-supported all edges using the NSGT and FSDPT are presented in this work. Four reinforcement types of CNTs along the length of nanoplates are considered, including UD, FG-O, FG-X, and FG-V. Based on the obtained results, several important conclusions can be drawn as follows:

- The frequencies of FG-CNTRC nanoplates increase as increasing the length-to-thickness ratio (a/h) or reducing the width-to-length ratio (b/a).
- The FG-CNTRC nanoplates arise the softening-stiffness effect as the nonlocal parameter (ea) is greater than the material length scale parameter (l); and arise the hardening-stiffness effect as the nonlocal parameter is smaller than the material length scale parameter.
- The CNT volume fraction (V_{CNT}^{*}) has an important impact on the vibration behavior of FG-CNTRC nanoplates. Specifically, increasing the CNT volume fraction leads to an increase in the frequencies of FG-CNTRC nanoplates. Moreover, among the distribution types of CNTs, FG-X causes the greatest increase in nanoplate's stiffness, while FG-O results in the weakest increase in nanoplate's stiffness. It means that the FG-X nanoplate has a maximum frequency and the FG-O nanoplate has a minimum frequency among FG-CNTRC nanoplates.

Author contributions

Conceptualization, DVH; methodology, DVH; software, NTKT; validation, DVH; formal analysis, DVH; investigation, NTKT; resources, DVH; data curation, DVH; writing—original draft preparation,

NTKT; writing—review and editing, DVH; visualization, NTKT; supervision, DVH; project administration, DVH; funding acquisition, DVH. All authors have read and agreed to the published version of the manuscript.

Conflict of interest

The authors declare that no conflict of interest.

References

1. Thostenson ET, Ren Z, Chou TW. Advances in the science and technology of carbon nanotubes and their composites: A review. *Composites Science and Technology* 2001; 61(13): 1899–1912. doi: 10.1016/s0266-3538(01)00094-x
2. Shen HS. Nonlinear bending of functionally graded carbon nanotube-reinforced composite plates in thermal environments. *Composite Structures* 2009; 91(1): 9–19. doi: 10.1016/j.compstruct.2009.04.026
3. Shen HS, Xiang Y. Nonlinear analysis of nanotube-reinforced composite beams resting on elastic foundations in thermal environments. *Engineering Structures* 2013; 56: 698–708. doi: 10.1016/j.engstruct.2013.06.002
4. Shen HS. Postbuckling of nanotube-reinforced composite cylindrical panels resting on elastic foundations subjected to lateral pressure in thermal environments. *Engineering Structures* 2016; 122: 174–183. doi: 10.1016/j.engstruct.2016.05.004
5. Shen HS, Wang H. Nonlinear vibration of compressed and thermally postbuckled nanotube-reinforced composite plates resting on elastic foundations. *Aerospace Science and Technology* 2017; 64: 63–74. doi: 10.1016/j.ast.2017.01.017
6. Zhu P, Lei ZX, Liew KM. Static and free vibration analyses of carbon nanotube-reinforced composite plates using finite element method with first order shear deformation plate theory. *Composite Structures* 2012; 94(4): 1450–1460. doi: 10.1016/j.compstruct.2011.11.010
7. Daikh AA, Houari MSA, Belarbi MO, et al. Analysis of axially temperature-dependent functionally graded carbon nanotube reinforced composite plates. *Engineering with Computers* 2021; 38(S3): 2533–2554. doi: 10.1007/s00366-021-01413-8
8. Liew KM, Lei ZX, Zhang LW. Mechanical analysis of functionally graded carbon nanotube reinforced composites: A review. *Composite Structures* 2015; 120: 90–97. doi: 10.1016/j.compstruct.2014.09.041
9. Zhang WM, Yan H, Peng ZK, et al. Electrostatic pull-in instability in MEMS/NEMS: A review. *Sensors and Actuators A: Physical* 2014; 214: 187–218. doi: 10.1016/j.sna.2014.04.025
10. Ghayesh MH, Farajpour A. A review on the mechanics of functionally graded nanoscale and microscale structures. *International Journal of Engineering Science* 2019; 137: 8–36. doi: 10.1016/j.ijengsci.2018.12.001
11. Eringen AC. Nonlocal polar elastic continua. *International Journal of Engineering Science* 1972; 10(1): 1–16. doi: 10.1016/0020-7225(72)90070-5
12. Eringen AC. On differential equations of nonlocal elasticity and solutions of screw dislocation and surface waves. *Journal of Applied Physics* 1983; 54(9): 4703–4710. doi: 10.1063/1.332803
13. Mindlin RD, Eshel NN. On first strain-gradient theories in linear elasticity. *International Journal of Solids and Structures* 1968; 4(1): 109–124. doi: 10.1016/0020-7683(68)90036-x
14. Mindlin RD. Second gradient of strain and surface-tension in linear elasticity. *International Journal of Solids and Structures* 1965; 1(4): 417–438. doi: 10.1016/0020-7683(65)90006-5
15. Yang F, Chong ACM, Lam DCC, et al. Couple stress based strain gradient theory for elasticity. *International Journal of Solids and Structures* 2002; 39(10): 2731–2743. doi: 10.1016/s0020-7683(02)00152-x
16. Lim CW, Zhang G, Reddy JN. A higher-order nonlocal elasticity and strain gradient theory and its applications in wave propagation. *Journal of the Mechanics and Physics of Solids* 2015; 78: 298–313. doi: 10.1016/j.jmps.2015.02.001
17. Shahriari B, Karamooz Ravari MR, Zeighampour H. Vibration analysis of functionally graded carbon nanotube-reinforced composite nanoplates using Mindlin's strain gradient theory. *Composite Structures* 2015; 134: 1036–1043. doi: 10.1016/j.compstruct.2015.08.118
18. Gia Phi B, Van Hieu D, Sedighi HM, et al. Size-dependent nonlinear vibration of functionally graded composite micro-beams reinforced by carbon nanotubes with piezoelectric layers in thermal environments. *Acta Mechanica* 2022; 233(6): 2249–2270. doi: 10.1007/s00707-022-03224-4
19. Daikh AA, Houari MSA, Belarbi MO, et al. Static and dynamic stability responses of multilayer functionally graded carbon nanotubes reinforced composite nanoplates via quasi 3D nonlocal strain gradient theory. *Defence Technology* 2022; 18(10): 1778–1809. doi: 10.1016/j.dt.2021.09.011

20. Hung PT, Thai CH, Phung-Van P. Isogeometric bending and free vibration analyses of carbon nanotube-reinforced magneto-electric-elastic microplates using a four variable refined plate theory. *Computers & Structures* 2023; 287: 107121. doi: 10.1016/j.compstruc.2023.107121